

Galerkin and Control Volume Finite Element Methods for Large Scale Air Pollution Simulations: a Comparison

Anton Antonov

Wolfram Research Inc.,
100 Trade Center Drive,
Champaign, IL 61820-7237, USA
e-mail: antonov@wolfram.com

Abstract

The methods compared – a Galerkin Finite Element Method (GFEM) and a Control Volume Finite Element Method (CVFEM) – are implemented within the object-oriented framework of the Danish Eulerian Model (DEM) for large scale air pollution simulations. The two methods are used to simulate incompressible advection dominated flows, in conjunction with a numerical ODE solver for the simulation of the chemistry reactions in DEM. Both methods are run over triangular grids and use linear basis functions. The GFEM and CVFEM mathematical formulations are explained in the paper. The results of the simulations are shown, and the corresponding GFEM and CVFEM phase and group velocities are discussed.

1 Introduction

In this paper we compare two methods for simulation of incompressible advection dominated flow used in conjunction with a numerical ODE solver for the simulation of the chemical reactions in the large scale air pollution model, called the Danish Eulerian Model (DEM)[8, 4, 10]. All important chemical species (sulfur pollutants, nitrogen pollutants, ammonia-ammonium, ozone, as well as many radicals and hydrocarbons) can be studied by DEM; its space domain contains the whole of Europe (the covered area is $4800\text{km} \times 4800\text{km}$). The methods are implemented within the object-oriented version of DEM, the Object-Oriented Danish Eulerian Model (OODEM)[3].

The first method is a Galerkin Finite Element Method (GFEM) with linear basis functions; the second method is a Control Volume Finite Element Method (CVFEM) with linear basis functions. Both methods are over triangular grids; (see Figure 1). They both are described in [5] by Gresho and Sani. In Section 2.2.6 of [5] is given a review of the control volume methods development (and literature). The CVFEM described in [5] is, as the authors state, “a fully legitimate (no cheating) *alternate finite element technique*” [5, Sec 2.2.6]. The most attractive property of the CVFEM is that it has the property of “local conservation” i.e. the conservation law is applied at control volume level. In this article, our goal is to judge what advantages or disadvantages CVFEM has compared with GFEM when applied in a large scale air pollution model like DEM. In Section 3 we will describe both methods, and compare their phase and group velocities. Tests and experiments with methods are presented in Section 4. The mathematical background for DEM is given in Section 2.

Another reason to make these comparisons is that it was relatively easy to do them. The OODEM is more than just a mathematical model implementation. It is a software framework, that makes the usual process of design, implementation, and testing of new methods 20 to 100 times faster[1, 2, 3].

2 Mathematical background of the Danish Eulerian Model

Temporal and spatial variations of the concentrations and/or the depositions of various harmful air pollutants can be studied [10] by solving the system (1) of partial differential equations (PDE's):

$$\begin{aligned}\frac{\partial c_s}{\partial t} &= -\frac{\partial(uc_s)}{\partial x} - \frac{\partial(vc_s)}{\partial y} - \frac{\partial(wc_s)}{\partial z} \\ &\quad + \frac{\partial}{\partial x}(K_x \frac{\partial c_s}{\partial x}) + \frac{\partial}{\partial y}(K_y \frac{\partial c_s}{\partial y}) + \frac{\partial}{\partial z}(K_z \frac{\partial c_s}{\partial z}) \\ &\quad + E_s + Q_s(c_1, c_2, \dots, c_q) - (k_{1s} + k_{2s})c_s, \\ s &= 1, 2, \dots, q.\end{aligned}\tag{1}$$

The different quantities that are involved in the mathematical model have the following meaning: (i) the concentrations are denoted by c_s ; (ii) u , v and w are wind velocities; (iii) K_x , K_y and K_z are diffusion coefficients; (iv) the emission sources in the space domain are described by the functions E_s ; (v) κ_{1s} and κ_{2s} are deposition coefficients; (vi) the chemical reactions used in the model are described by the non-linear functions $Q_s(c_1, c_2, \dots, c_q)$. The number of equations q is equal to the number of species that are included in the model.

It is difficult to treat the system of PDE's (1) directly. This is the reason for using different kinds of splitting. A simple splitting procedure, based on ideas discussed in Marchuk[6] and McRae et al. [7], can be defined, for $s = 1, 2, \dots, q$, by the following sub-models:

$$\frac{\partial c_s^{(1)}}{\partial t} = -\frac{\partial(uc_s^{(1)})}{\partial x} - \frac{\partial(vc_s^{(1)})}{\partial y}\tag{2}$$

$$\frac{\partial c_s^{(2)}}{\partial t} = \frac{\partial}{\partial x}\left(K_x \frac{\partial c_s^{(2)}}{\partial x}\right) + \frac{\partial}{\partial y}\left(K_y \frac{\partial c_s^{(2)}}{\partial y}\right)\tag{3}$$

$$\frac{dc_s^{(3)}}{dt} = E_s + Q_s(c_1^{(3)}, c_2^{(3)}, \dots, c_q^{(3)})\tag{4}$$

$$\frac{dc_s^{(4)}}{dt} = -(\kappa_{1s} + \kappa_{2s})c_s^{(4)}\tag{5}$$

$$\frac{\partial c_s^{(5)}}{\partial t} = -\frac{\partial(wc_s^{(5)})}{\partial z} + \frac{\partial}{\partial z}\left(K_z \frac{\partial c_s^{(5)}}{\partial z}\right)\tag{6}$$

The horizontal advection, the horizontal diffusion, the chemistry, the deposition and the vertical exchange are described with the system (2)-(6). This is not the only way to split the model defined by (1), but the particular splitting procedure (2)-(6) has three advantages: (i) the physical processes involved in the big model can be studied separately; (ii) it is easier to find optimal (or, at least, good) methods for the simpler systems (2)-(6) than for the big system (1); (iii) if the model is to be considered as a two-dimensional model, then one should just skip system (6). The methods and the tests in the article are for the two-dimensional model, i.e. for the system (2)-(5).

Remark The functions c_s , u , v , K_x , K_y are space and time dependent, e.g. $c_s = c_s(x, y, t)$.

3 Description of the methods, theoretical comparison

The two-dimensional advection-diffusion submodel of DEM is described just by equations (2) and (3). Hence we can omit the species index s , since the equations are identical for all s . Also, in DEM the

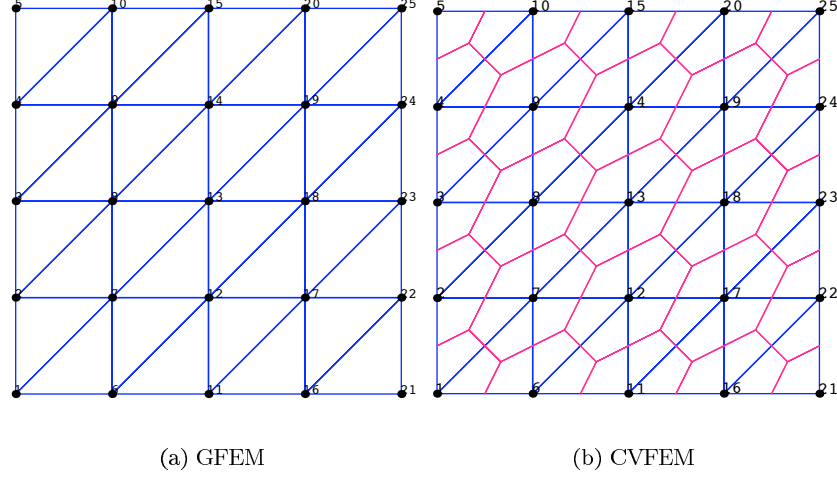


Figure 1: Parts of the grids on which the tests and experiments were made. The tests/experiments grids have 96×96 nodes.

diffusion coefficients K_x and K_y are constants. With GFEM and CVFEM the advection and diffusion are treated together, so we can combine (2) and (3), and obtain (index s omitted):

$$\frac{\partial c}{\partial t} = -\frac{\partial(uc)}{\partial x} - \frac{\partial(vc)}{\partial y} + K_x \frac{\partial^2 c}{\partial x^2} + K_y \frac{\partial^2 c}{\partial y^2}. \quad (7)$$

We will consider the numerical solution of (7) over the two dimensional area Ω with boundary Γ . All space dependent functions considered will have domain that coincides with Ω . With $Supp(f)$ we will denote the support of the function f . When Ω is covered with a finite element grid, the set of the grid elements will be denoted with E , the set of the grid nodes with I . Let $\bigcup_{j=1}^{|E|} e_j = E$, and $\{1, \dots, |I|\} = I$. With $\varphi_j = \varphi_j(x, y)$ and $\psi_j = \psi_j(x, y)$ we will denote the basis and test function at node j respectively. With E_j we will denote the minimal set of elements that contains $Supp(\varphi_j)$. The support of any basis or test function is a proper subset of Ω .

3.1 Galerkin Finite Element Method

In GFEM, from (7) we make the week formulation by multiplying (7) by a test function φ_j and integrating over the φ_j 's domain, that coincides with Ω for every j :

$$\int_{\Omega} \frac{\partial c}{\partial t} \varphi_j = \int_{\Omega} \left(-\frac{\partial(uc)}{\partial x} - \frac{\partial(vc)}{\partial y} + K_x \frac{\partial^2 c}{\partial x^2} + K_y \frac{\partial^2 c}{\partial y^2} \right) \varphi_j, \quad j = 1, \dots, |I|.$$

Next we substitute $c(x, y, t)$ with the expansion $c(x, y, t) = \sum_{i=1}^{|I|} g_i(t) \varphi_i(x, y)$:

$$\begin{aligned} & \sum_{i=1}^{|I|} \frac{\partial g_i}{\partial t} \int_{\Omega} \varphi_i \varphi_j = \\ & \sum_{i=1}^{|I|} g_i \int_{\Omega} \left(-\frac{\partial(u\varphi_i)}{\partial x} \varphi_j - \frac{\partial(v\varphi_i)}{\partial y} \varphi_j + K_x \frac{\partial \varphi_i}{\partial x} \frac{\partial \varphi_j}{\partial x} + K_y \frac{\partial \varphi_i}{\partial y} \frac{\partial \varphi_j}{\partial y} \right), \\ & j = 1, \dots, |I|. \end{aligned}$$

If $I_j = \{i : \text{Supp}(\varphi_i) \cap \text{Supp}(\varphi_j) \neq \emptyset\}$ we can rewrite the last equation as

$$\begin{aligned} \sum_{i \in I_j} \frac{\partial g_i}{\partial t} \int_{E_j} \varphi_i \varphi_j = \\ \sum_{i \in I_j} g_i \int_{E_j} \left(-\frac{\partial(u\varphi_i)}{\partial x} \varphi_j - \frac{\partial(v\varphi_i)}{\partial y} \varphi_j + K_x \frac{\partial\varphi_i}{\partial x} \frac{\partial\varphi_j}{\partial x} + K_y \frac{\partial\varphi_i}{\partial y} \frac{\partial\varphi_j}{\partial y} \right), \\ j = 1, \dots, |I|. \end{aligned} \quad (8)$$

If we define the numbers

$$\begin{aligned} p_{ji} &= \int_{E_j} \varphi_i \varphi_j, \\ a_{ji} &= \int_{E_j} \left(-\frac{\partial(u\varphi_i)}{\partial x} \varphi_j - \frac{\partial(v\varphi_i)}{\partial y} \varphi_j + K_x \frac{\partial\varphi_i}{\partial x} \frac{\partial\varphi_j}{\partial x} + K_y \frac{\partial\varphi_i}{\partial y} \frac{\partial\varphi_j}{\partial y} \right), \end{aligned}$$

then (8) can be written as

$$\sum_{i \in I_j} \frac{\partial g_i}{\partial t} p_{ji} = \sum_{i \in I_j} g_i a_{ji}, \quad j = 1, \dots, |I|,$$

which is equivalent to

$$P \frac{\partial \vec{g}(t)}{\partial t} = A \vec{g}(t), \quad (9)$$

where $P = \{p_{ji}\}$, $A = \{a_{ji}\}$, $i, j = 1, \dots, \dim(S)$, $\vec{g}(t) \in \mathbf{R}^{|I|}$. So the problem to solve approximately (7) is reduced to the problem of solving the system of ODE's (9).

3.2 Control Volume Finite Element Method

In CVFEM we partition Ω into non-overlapping regions in a manner shown with the red contours on Figure 1. Each of these regions surrounds exactly one node. So, if a region surrounds the node j , it will be denoted as Ω_j . To each Ω_j we will assign a corresponding test function ψ_j that is 1 within Ω_j and 0 outside of Ω_j . The boundary of Ω_j will be denoted as Γ_j .

In CVFEM, we make the week formulation by multiplying (7) by a test function ψ_j and integrating over the ψ_j 's domain, that coincides with Ω for every j :

$$\int_{\Omega} \frac{\partial c}{\partial t} \psi_j = \int_{\Omega} \left(-\frac{\partial(uc)}{\partial x} - \frac{\partial(vc)}{\partial y} + K_x \frac{\partial^2 c}{\partial x^2} + K_y \frac{\partial^2 c}{\partial y^2} \right) \psi_j, \quad j = 1, \dots, |I|.$$

But owing to the definition of the test functions, and using the divergence theorem, the above equation is equivalent to

$$\int_{\Omega_j} \frac{\partial c}{\partial t} = \int_{\Omega_j} \vec{n} \cdot (-\vec{W}c + \nabla(\vec{k}c)), \quad j = 1, \dots, |I|,$$

where $\vec{W} = \begin{bmatrix} u \\ v \end{bmatrix}$, $\vec{k} = \begin{bmatrix} K_x \\ K_y \end{bmatrix}$. Next, as in GFEM, we substitute $c(x, y, t)$ with the expansion $c(x, y, t) = \sum_{i=1}^{|I|} g_i(t) \varphi_i(x, y)$:

$$\sum_{i=1}^{|I|} \frac{\partial g_i}{\partial t} \int_{\Omega_j} \varphi_i = \sum_{i=1}^{|I|} g_i \int_{\Gamma_j} \vec{n} \cdot (-\vec{W} \varphi_i + \nabla(\vec{k} \varphi_i)), \quad j = 1, \dots, |I|.$$

If $I_j = \{i : \text{Supp}(\varphi_i) \cap \text{Supp}(\psi_j) \neq \emptyset\} = \{i : \text{Supp}(\varphi_i) \cap \Omega_j \neq \emptyset\}$ we can rewrite the last equation as

$$\sum_{i \in I_j} \frac{\partial g_i}{\partial t} \int_{\Omega_j} \varphi_i = \sum_{i \in I_j} g_i \int_{\Gamma_j} \vec{n} \cdot (-\vec{W} \varphi_i + \nabla(\vec{k} \varphi_i)), \quad j = 1, \dots, |I|. \quad (10)$$

3.2.1 Implementational remarks

- The computation of the right hand side integral of (10) can be done in two ways. Let $E_j = \{k : e_k \in E \wedge e_k \cap \Omega_j \neq \emptyset\}$. It is natural to assume that the wind field $\vec{W} = \vec{W}(x, y, t)$ is given at the nodes of the grid. We can assume further that the wind is constant within the elements. Let \vec{W}_i denote the wind at node i , and let \vec{W}_{e_i} denotes the constant wind within the element $e_i \in E$. Then the right hand side integral of (10),

$$\int_{\Gamma_j} \vec{n} \cdot (-\vec{W}\varphi_i + \nabla(\vec{k}\varphi_i)),$$

can be computed either with the formula

$$\int_{\Gamma_j} \vec{n} \cdot (-\vec{W}_j\varphi_i + \nabla(\vec{k}\varphi_i)), \quad (11)$$

or with the formula

$$\sum_{k \in E_j} \int_{\Gamma_j \cap e_k} \vec{n} \cdot (-\vec{W}_{e_k}\varphi_i + \nabla(\vec{k}\varphi_i)). \quad (12)$$

- The red contours in Figure 1-(b) are drawn between the midpoints of the blue triangles.

3.3 Phase and group velocities

If we consider the methods with constant wind field on infinite regular grids for the model equation

$$\frac{\partial c}{\partial t} = -W \cos \phi \frac{\partial c}{\partial x} - W \sin \phi \frac{\partial (vc)}{\partial y}, \quad (13)$$

we can derive their phase and group velocities. This was done using a Fourier analysis technique described by Vichnevetsky in [9]; a description how this technique was applied to GFEM in OODEM can be found in [3]. With this technique we find the numerical velocity W^* that corresponds to W when solving (13). The corresponding GFEM and CVFEM phase and group velocities for the grids on Figure 1 are shown on Figure 2.

We can make the following observations:

- we can see the famous anisotropy property of the triangle meshes: short-length waves propagate faster in the direction perpendicular to the triangles hypotenuses;
- GFEM has more isotropical phase velocities;
- for both methods the negative group velocities of the $2\Delta x$ wave (see [5, Sec. 2.6] or [3, Ch. 3]) are very anisotropic, and they have similar shapes; (these are the “butterfly” contours;)
- the amplitude of the negative group velocity ratio of the CVFEM $2\Delta x$ wave is 2, and that of GFEM is 3. This is in agreement with the observation in [5, p. 149] that “the *higher* the phase accuracy is for long waves [...], the *larger* is the negative short-wave group velocity”;

4 Tests and experiments, practical comparisons

4.1 Rotational tests

For both methods we can do the pure-advection rotational test [10]. of cone concentration distribution. The results of this test, over the 96×96 grids shown on Figure 1, are shown on Figure 3. The CVFEM

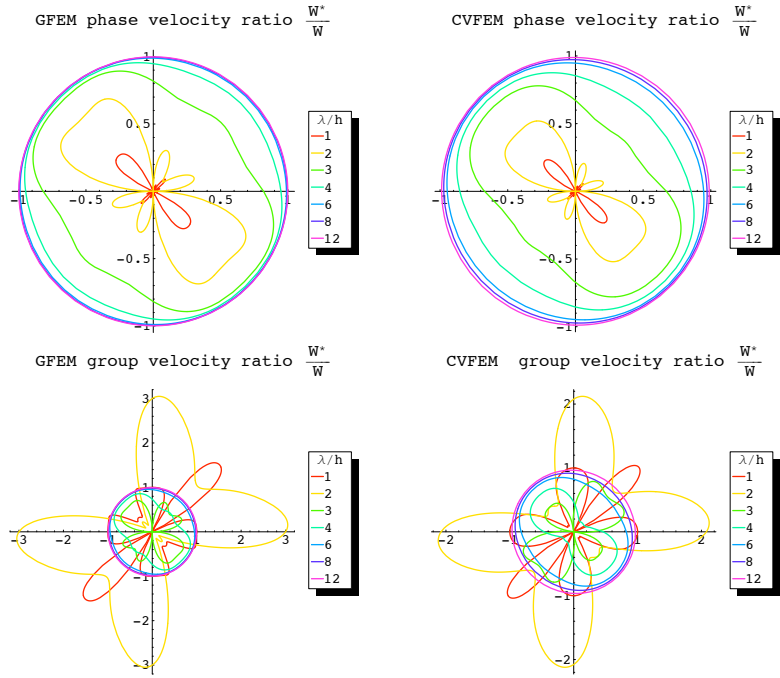


Figure 2: Phase and group velocities for GFEM and CVFEM for the grids on Figure 1. The velocities are computed for the Currant number $W\Delta t/h = 0.2$.

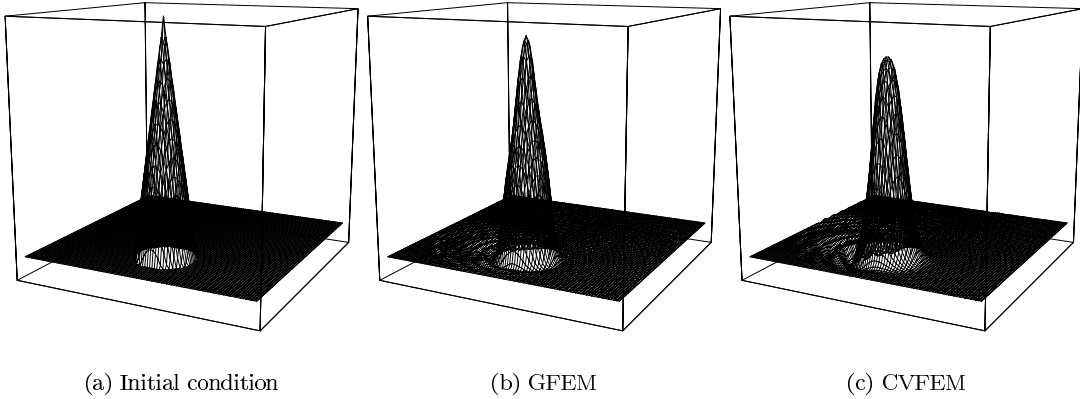
cone is more “dumped”, which fits the prediction by the phase velocity graphics on Figure 2. Both formulas (11) and (12) were used for the CVFEM scheme. The results are almost identical: the cone heights are 83.9175 and 83.9173 for (11) and (12) respectively. The number of iterations on each step are 2 and 3 for CVFEM and GFEM respectively.

4.2 Experiments with real data

Three simulations were made with the following methods/implementations:

1. GFEM
2. CVFEM with formula (11)
3. CVFEM with formula (12)

All simulations were made for July 1995 with the data set used in DEM at the National Environmental Research Institute (NERI) of Denmark. The 96×96 grids used are shown on Figure 1. The quality of the simulations can be judged with scatter plots, like those shown on Figure 4. The scatter plots are made with the measurements of pollutants for the given period (July'95) and the simulation results. The correspondence between the measurements and the simulation results are summarized on Figure 5. We can see from these figures that CVFEM with formula (12) produces results very close to those by the GFEM method. We did some additional visualizations that suggest to “rule out” CVFEM with formula (11) – it does not produce expected results. Further experiments/comparisons should be done.

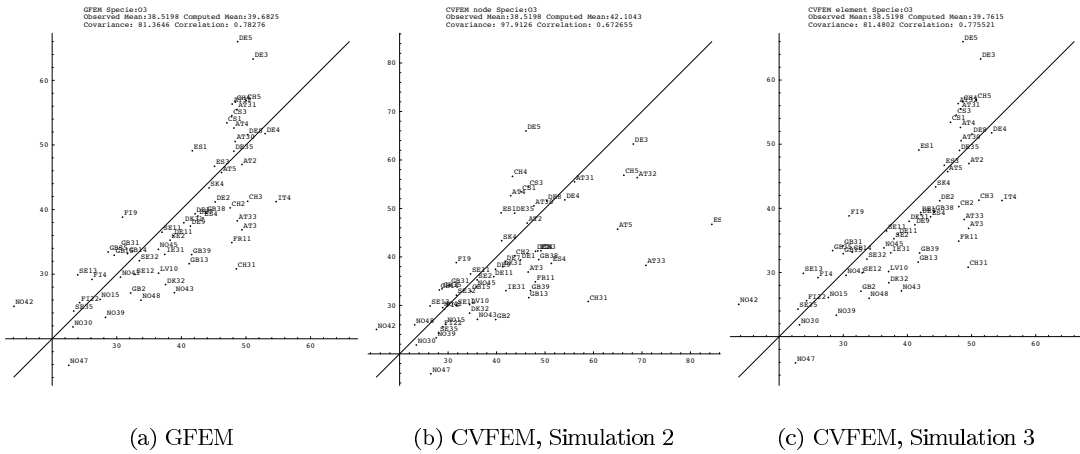


(a) Initial condition

(b) GFEM

(c) CVFEM

Figure 3: Rotational tests initial condition and results after one rotation for GFEM and CVFEM. The height of the initial condition cone is 100, the height of the GFEM cone is 92.33, the height of the CVFEM cone is 83.92.



(a) GFEM

(b) CVFEM, Simulation 2

(c) CVFEM, Simulation 3

Figure 4: Scatter plots for O_3 simulated(x -axis) vs. measured(y -axis) July'95.

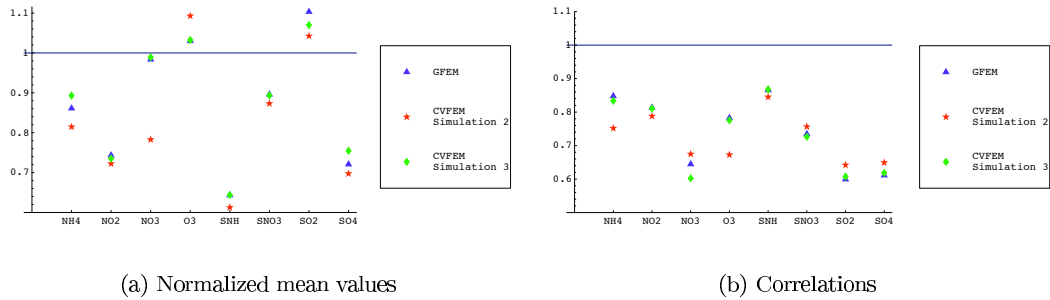


Figure 5: Results from simulations 1, 2, and 3. On picture (a) the mean of monthly averaged computed values are divided by the observed mean. On picture (b) are the correlations of the monthly averaged computed values and averaged observed values.

5 Conclusions and future plans

The main goal of the article was to compare a theoretically correct CVFEM – as described in [5] – with GFEM for a time dependent simulation of an advection dominated flow. The presented theoretical results were obtained with simplifying assumptions, and the presented experimental results are done for just one month. From the theoretical and test results we can conclude that (i) CVFEM is inferior to GFEM within the framework of the Danish Eulerian Model. From the experimental result we can conclude that (ii) if GFEM or CVFEM wins over the other, it will be within “a narrow” margin. (It is predicted in [5] that GFEM would win within “a narrow” margin.) More experiments should be done. These additional experiments should be done for a large number of months in different years. It will be nice if the experiments are repeated with different chemical schemes/solvers.

Other extensions of the work presented can be a similar comparisons with regular rectangular grids and comparisons with grids with local refinements. (The later might include tests how CVFEM propagates waves through inner boundaries of local refinements; see [3] about GFEM.) It will be also interesting to see how the theoretically obtained phase velocities fit the rotational tests results.

References

- [1] Anton Antonov. Framework for parallel simulations in air pollution modeling with local refinements. 2001.
- [2] Anton Antonov. Object-oriented framework for large scale air pollution modeling. In Svetozar Margenov, Jerzy Wasniewski, and Plamen Y. Yalamov, editors, *Large-Scale Scientific Computing, Third International Conference, LSSC 2001, Sozopol, Bulgaria, June 6-10, 2001, Revised Papers*, volume 2179 of *Lecture Notes in Computer Science*, pages 247–254. Springer, June 2001. <http://link.springer.de/link/service/series/0558/tocs/t2179.htm>.
- [3] Anton Antonov. *Object-Oriented Framework for Large Scale Air Pollution Models*. PhD thesis, The Technical University of Denmark, April 2001.
- [4] A. Bastrup-Birk, J. Brandt, I. Uria, and Z. Zlatev. Studying cumulative ozone exposures in europe during a 7-year period. *Journal of Geophysical Research*, 102:23917–23935, 1997.
- [5] P. M. Gresho and R. L. Sani. *Incompressible Flow and Finite Element Method*. John Wiley and Sons, 1998.
- [6] G. I. Marchuk. *Methods for Numerical Mathematics*. Springer-Verlag, 2 edition, 1982.
- [7] G. McRae, W. R. Goodin, and J. H. Seinfeld. Numerical solution of the atmospheric diffusion equation for chemically reacting flows. *Journal of Computational Physics*, 45(1):356–396, 1982.
- [8] C. Ambelas Skjøth, A. Bastrup-Birk, J. Brandt, and Z. Zlatev. Studying variations of pollution levels in a given region of europe during a long time-period. *Systems Analysis Modelling Simulation*, 37:297–311, 2000.
- [9] R. Vichnevetsky and J. B. Bowles. *Fourier Analysis of Numerical Approximations of Hyperbolic Equations*. SIAM, 1982.
- [10] Z. Zlatev. *Computer Treatment of Large Air Pollution Models*. Kluwer, 1995.